Correlation of MR Perfusion Imaging and Vessel Tortuosity Parameters in Assessment of Intracranial Neoplasms

Anup H. Parikh, B.S.[1], **J. Keith Smith, M.D., Ph.D.**[2,*], **Matthew G. Ewend, M.D.**[3], and **Elizabeth Bullitt, M.D.**[3]

1 *School of Medicine, University of North Carolina School of Medicine 3327 Old Infirmary CB 7510 Chapel Hill, NC 27599-7510 USA*

2 *Department of Radiology, University of North Carolina School of Medicine 3327 Old Infirmary CB 7510 Chapel Hill, NC 27599-7510 USA*

3 *Department of Surgery, University of North Carolina School of Medicine 3327 Old Infirmary CB 7510 Chapel Hill, NC 27599-7510 USA*

Abstract

Advances in noninvasive imaging techniques such as magnetic resonance perfusion imaging have been found useful in grading cerebral neoplasms and have potential for significant clinical benefit. The purpose of this study was to determine the correlation between tumor vessel tortuosity as measured from vessels extracted from magnetic resonance angiograms (MRA) and perfusion parameters of cerebral blood flow (CBF) and cerebral blood volume (CBV) in intracranial neoplasms. We hypothesized that tumor blood vessel tortuosity measures and perfusion measures would be correlated, since both are increased by tumor angiogenesis. 18 patients with 19 cerebral neoplasms were evaluated with conventional MR imaging and dynamic contrast-enhanced T2-weighted perfusion MR imaging (PWI). Both benign and malignant lesions were included, as were hyper- and hypovascular tumors. Regions of interest were plotted within the tumor area to locate foci of maximum CBV and CBF. CBV and CBF measurements were also recorded in contralateral normal appearing white matter to calculate relative CBV (rCBV) and relative CBF (rCBF). Vessel tortuosity analyses were conducted upon vessels segmented from MRA images of the same patients using two tortuosity descriptors (SOAM and ICM), which have previously been demonstrated to have efficacy in separating benign from malignant disease. Linear regression analyses were conducted to determine if correlations exist between CBV or CBF and the two tortuosity measurements. For the overall set of tumors, no significant correlations were found between flow or volume measures and the tortuosity measures. However, when the 7 glioblastoma multiforme tumors were examined as a subgroup, the following significant correlations were found: rCBV and SOAM (R^2=0.799), rCBV and ICM (R^2=0.214). Our results demonstrate that MR perfusion imaging data do not correlate significantly with vessel tortuosity parameters as determined from the larger vessels seen by MRA. However, for subgroups of a particular tumor type such as GBM, there may be significant correlations. It appears that perfusion and tortuosity data may provide independently useful data in the assessment of cerebral neoplasms.

Introduction

Advances in noninvasive imaging techniques such as perfusion MR imaging have been found useful in grading cerebral neoplasms and have potential for significant clinical benefit (1–7). An alternative approach is to analyze shape measures of the larger vessels seen by magnetic

* Corresponding Author: J. Keith Smith, M.D., Ph D. Email: jksmith@med.unc.edu.

resonance angiography (MRA). This approach also has been shown to have potential for discriminating between benign and malignant disease (8–10). In this study, we attempt to determine the independent utility of perfusion MR imaging and the morphologic analysis of the larger vessels visualized directly by MRA for evaluation of intracranial neoplasms.

The advantage of perfusion imaging is that it can provide information at the sub-voxel level. The disadvantage of perfusion imaging is that it is restricted to analysis of blood flow and volume, and both malignant and benign tumors may be either hypo- or hypervascular. An assessment of malignancy based solely upon perfusion measures may therefore provide a significant number of both false positives and false negatives (7).

Analysis of the larger vessels seen by MRA has complementary advantages and disadvantages. The disadvantage of analysis of these larger vessels is that current levels of MRA resolution preclude direct imaging of capillaries, and so important information may be missed. The advantage of analyzing the larger vessels seen by MRA is that multiple shape measures can be assessed in addition to that of blood vessel density. In particular, abnormal vessel tortuosity is known to be associated with malignancy (11–13), Indeed, a prior blinded study aimed at discriminating between benign and malignant tumors was successful in classifying all tumors correctly based upon the tortuosity measurements of vessels defined from MRA and located in the vicinity of each tumor (10).

The purpose of the current study is to investigate if there exists a correlation between cerebral blood volume and flow with direct measurements of vessel tortuosity. This analysis would help determine whether diagnostic workup of cerebral neoplasms is augmented by both macroscopic vessel analysis and perfusion parameters of flow and volume. It is our hypothesis that tumor blood vessel tortuosity measures and perfusion measures should be correlated, since both are likely to increase as a result of tumor angiogenesis.

Materials and Methods

18 patients with 19 cerebral neoplasms (primary astrocytic brain neoplasms included glioblastoma multiforme [7], low grade glioma [1], grade 3 anaplastic astrocytoma [1], and grade 2 astrocytoma [1]; other neoplasms included metastases [6], pituitary adenoma [1], lymphoma [1], and oligodendroglioma [1]) were evaluated with conventional MR imaging and dynamic contrast-enhanced T2-weighted perfusion MR imaging (PWI). Images were obtained on either a head-only 3T MR unit (Allegra, Siemens Medical Systems, Inc., Germany) or upon a 1.5T MR unit (Sonata, Siemens Medical Systems Inc., Germany). A quadrature head coil was employed. T1, T2, and MRA sequences were performed on all subjects.

A localizing sagittal T1-weighted image was obtained followed by non-enhanced axial T1-weighted (600/14 [TR/TE]), axial fluid-attenuated inversion-recovery (FLAIR, 9000/110/2500 [TR/TE/TI]), and T2-weighted (3400/119) images. Contrast material-enhanced axial T1-weighted imaging was performed after the acquisition of the perfusion MR imaging data.

Dynamic contrast agent-enhanced T2-weighted gradient-echo echo-planar images were acquired during the first pass of a standard dose (0.1 mmol/kg) bolus of gadopentalate dimeglumine. (Magnevist; Berlex Laboratories, Wayne, NJ).

Vascular images employed a 3D time-of-flight MRA sequence. Our methods require visualization of tiny vessels, voxels that are close to isotropic, and inclusion of the entire head. Images were acquired using a protocol of $352 \times 448 \times 176$ voxels and a voxel size of $0.5 \times 0.5 \times 0.8$ mm^3. Velocity compensation along both frequency and phase encoding directions was used to minimize signal dephasing induced by the flowing spins. A magnetization transfer

saturation pulse was applied to suppress signal from stationary brain parenchyma, augmenting vascular contrast.

Image Processing: Large Vessels Seen by MRA

The approach is based upon a statistical analysis of blood vessel attributes (vessel shape and density measures). For each tumor patient, a region of interest is defined. This region is usually the tumor volume as seen by gadolinium-enhanced T1 images, but for tiny or avascular tumors the region of interest is dilated until it includes a minimum of four vessels. This region of interest is then mapped to the same patient's MRA as well as to the MRAs of 17 healthy subjects. Multiple measures of vessel shape are then calculated for all subjects within the corresponding region of interest, and the tumor patient's values are normalized *via* z-score by the means and standard deviations of the values obtained from the healthy subjects. This approach requires: i) a method of vessel definition, ii) a method of tumor definition, iii) a method of aligning (registering) images, and iv) a set of methods to define significant vessel attributes.

Vessel segmentation was done by Aylward's method (14). Vessel extraction involves 3 steps: definition of a seed point, automatic extraction of an image intensity ridge representing the vessel's central skeleton, and automatic determination of vessel radius at each skeleton point. The output of the program provides sets of directed, 4-dimensional points indicating the (x,y,z) spatial position of each sequential vessel skeleton point and an associated radius at each point. Extracted vessels were then post-processed to produce connected vessel trees and to exclude noise (15).

Tumor segmentation was performed using either a fully automated method (16) or a partially manual program that segments tumors via polygon drawing and filling on orthogonal cuts through an image volume (www.cs.unc.edu/~gerig/).

All images were registered via a mutual-information based, affine transformation (17,18) into the coordinate system of the McConnell atlas (19) so that, via a combination of forward and backward mapping, the same region of interest could be defined within each image. For each tumor patient, vessels were automatically clipped to the tumor margins and an automated analysis of vessel shape was performed only upon those vessels lying within the tumor boundaries. This same region of interest was then mapped into the coordinate space of each healthy patient, and a similar, regional analysis was performed upon each healthy subject's vasculature.

For purposes of malignancy classification based upon vessel shape measures, we have found tortuosity determination to be the most important factor (10). We have previously described two tortuosity measures (9). The "Sum of Angles Metric" (SOAM) sums total curvature along a space curve and normalizes by path length. The SOAM is effective in detecting high-frequency, low-amplitude sine waves or coils. The "Inflection Count Metric" (ICM) counts minima of curvature along a space curve and then multiplies this number (plus 1) times the total path length and divides by the distance between endpoints. The ICM is effective in detecting vessels in an abnormal "bag of worms" configuration. Malignant tumor vessels almost invariably exhibit abnormalities detectable by SOAM and, if foci of detectable

Image Processing: Perfusion Measures

For the CBF and CBV data, regions of interest (ROI) were plotted within the tumor area to locate foci of maximum flow and volume. CBV and CBF measurements were also recorded in contralateral normal appearing white matter to calculate relative CBV (rCBV) and relative CBF (rCBF). The methods for acquiring perfusion data from a set of dynamic contrast-

enhanced echo-planar images and the precise algorithm for calculating rCBV and rCBF have been previously described (1).

Analysis—Linear regression analyzes were conducted to determine if correlations exist between CBV or CBF and the two parameters used to measure the shapes of the larger vessels seen directly by MRA.

Results

CBF, CBV and vessel tortuosity parameters of SOAM and ICM were collected for 19 tumors. Correlation analysis results of CBF, CBV and the tortuosity parameters are shown in Table I.

No significant correlations were found between flow or volume measures and the two tortuosity parameters (Table I). Subgroup analyzes were also conducted to examine the primary astrocytic neoplasms; however, no significant correlations were found. When examining the glioblastoma multiforme tumors as a subgroup, however, the following significant correlations were found: rCBV and SOAM (R^2=0.799), rCBV and ICM (R^2=0.214). Figure 1(a–d) illustrates the linear correlations between the perfusion and tortuosity parameters.

Analyzing the distribution of nlCBF, nlCBV, SOAM, and ICM stratified by tumor grade (benign, low, high) was also informative. With respect to nlCBV, the high grade tumors as a group had a higher mean value than the low grade group. It is interesting to note that the benign group had a mean similar to the high grade group. This is not a surprising finding as benign tumors such as meningiomas are known to have high flow and volume. With respect to nlCBF, the high grade group has a higher mean value than the low grade group. The benign group had a mean value approximately equal to the low grade group. With respect to SOAM, the benign group had the highest mean value followed by approximately equal mean values for the low and high grade groups. For ICM, the high grade group had the highest mean value. The low grade group had the lowest value while the benign group was intermediate.

Discussion

Grading of cerebral neoplasms with noninvasive diagnostic imaging techniques has potential for significant clinical benefit. To date however, it has yet to be demonstrated as a reliable process with high sensitivity and specificity. Although noninvasive imaging approaches to detect malignancy have included positron emission tomography, and magnetic resonance (MR) spectroscopy, perfusion MR, and diffusion weighted MR images, as well as various image processing methods, a single method has yet to be proven fully reliable in differentiating benign from malignant disease (24–32).

In evaluating cerebral neoplasms, especially gliomas, there are significant limitations associated with histopathologic grading. There is inherent sampling error associated with stereotactic biopsy and also the inability to properly evaluate residual tumor tissue after cryoreductive surgery (33). The advantage of novel MR imaging techniques in evaluating cerebral neoplasms is the ability to sample not only the entire lesion, but also the adjacent tissue for physiologic changes.

Conventional MR imaging with contrast agents is already an established, useful tool in characterization of cerebral tumors, especially in terms of anatomy and morphology (34–38). However, in terms of classifying and grading tumors with optimization sequences and protocols, no method has proven to be very reliable. The sensitivity for glioma grading has been shown to range from 55.1% to 83.3% (1,39–42). Much of this reduced sensitivity is due

to the fact that not all high grade lesions manifest with the typical characteristics of contrast enhancement, edema, hemorrhage, necrosis, and/or mass effect.

Dean *et al.* demonstrated that the two most important predictors of tumor grade are mass effect and necrosis (43). The dilemma lies in the situation when a high grade glioma is mistaken for being low grade due to minimal edema, no contrast enhancement, no necrosis, and no mass effect. On the other hand, low-grade gliomas can be mistaken for being high grade due to peritumoral edema, contrast enhancement, central necrosis, and mass effect. Several studies have demonstrated that contrast material enhancement alone is not always accurate in predicting tumor grade (44–46). Also, when using conventional T2-weighted MR images, the peritumoral hyperintensity is nonspecific as it may represent vasogenic edema, tumor infiltration, or both. Moreover, conventional MR imaging does not provide reliable information on tumor physiology which is a significant factor in determining tumor grade.

Recently, advanced imaging techniques such as perfusion MR imaging and proton MR spectroscopy have been found useful in studying brain tumors. Specifically, relative cerebral blood volume (rCBV) maps and measurements have been shown to correlate with tumor grade and histologic findings of increased tumor vascularity (20–23). It is plausible that physiological measurements such as blood volume and flow would assist in predicting tumor grade. Despite the widespread interest in characterization of neoplasms with perfusion MR imaging, the current clinical role of CBV and CBF (cerebral blood flow) requires further investigation.

In addition to the parameters of blood flow and volume, another characteristic of interest is vessel tortuosity. It has been demonstrated in previous studies that neoangiogenesis associated with malignancy often results in vessels distinguished by a tortuous shape (11–13). This observation led to investigation of whether high-resolution MRA analysis of vessel shape could be used for noninvasive diagnosis of malignancy.

Discrete definition of vessel paths is key in studying vessel tortuosity. The most common approach to visualizing vessels in 3D is by maximum intensity projection, which allows inspection of a block of data from any point of view. Previous investigators have proposed methods of mathematically defining vessels from 3D image data (47). In the approach from our institution, the advantage is definition of very small vessels without significant noise interference. The exact meaning of vessel tortuosity is not standard by any means. A recent proposed classification scheme of "abnormal tortuosity" is comprised of three different patterns (9). Tortuosity type I occurs when a straight vessel elongates to form a "C" or "S", and occurs with retinopathy of prematurity, anemia, and hypertension. Tortuosity type II is characterized by a "can of worms" configuration, and occurs within many hypervascular lesions. Tortuosity type III is characterized by high-frequency, low-amplitude coils or sine waves, and appears within malignant tumors.

This report provides insight into two novel noninvasive methods of determining tumor malignancy. Both methods have previously been described in separate reports to be significant predictors of tumor grade and to augment conventional diagnostic imaging techniques. We specifically intended to study whether there exists a correlation between the MR perfusion parameters of CBF and CBV and the parameters of vessel tortuosity analysis. Our premise was that if both parameters are correlated, then one method would suffice as part of the diagnostic workup of cerebral neoplasms. Our results demonstrate that the MR perfusion imaging data do not correlate significantly with vessel tortuosity parameters. This may be due to the fact that tortuosity does not depend on vessel density. However when stratified by grade, the high grade tumors in our study had higher mean values with respect to nlCBF, nlCBV, SOAM, and ICM than the low grade tumors. For subgroups of tumors such as GBM, there may be significant correlations and further investigation with larger sample size would need to be undertaken to

determine this. Overall, it appears that the perfusion and tortuosity data may both provide independently useful data in the assessment of cerebral neoplasms.

References

1. Knopp EA, Cha S, Johnson G, et al. Glial Neoplasms: Dynamic Contrast-enhanced T2*-weighted MR Imaging. Radiology 1999;211:791–798. [PubMed: 10352608]

2. Wong JC, Provenzale JM, Petrella JR. Perfusion MR Imaging of Brain Neoplasms. Am J Roentgenol 2000;174:1147–1157. [PubMed: 10749268]

3. Cha S, Knopp EA, Johnson G, et al. Intracranial Mass Lesions: Dynamic Contrast-enhanced Susceptibility-weighted Echo-planar Perfusion MR Imaging. Radiology 2002;223:11–29. [PubMed: 11930044]

4. Lev MH, Rosen BR. Clinical Applications of Intracranial Perfusion MR Imaging. Neuroimaging Clin N Am 1999;9:309–331. [PubMed: 10318717]

5. Shin JH, Lee HK, Kwun BD, et al. Using Relative Cerebral Blood Flow and Volume to Evaluate the Histopathologic Grade of Cerebral Gliomas: Preliminary Results. Am J Roentgenol 2002;179:783–789. [PubMed: 12185064]

6. Petrella JR, Provenzale JM. MR Perfusion Imaging of the Brain: Techniques and Applications. Am J Roentgenol 2000;175:207–219. [PubMed: 10882275]

7. Law M, Yang S, Wang H, Babb JS, Johnson G, Cha S, Knopp EA, Zagzag D. Glioma Grading: Sensitivity, Specificity, and Predictive Values of Perfusion MR Imaging and Proton MR Spectroscopic Imaging Compared with Conventional MR Imaging. AJNR 2003;24:1989–1998. [PubMed: 14625221]

8. Bullitt E, Gerig G, Aylward S, Joshi S, Smith K, Ewend M, Lin W. Vascular Attributes and Malignant Brain Tumors. MIC-CAI 2003 Lecture Notes in Computer Science 2003;2878:671–679.

9. Bullitt E, Gerig G, Pizer S, Aylward SR. Measuring Tortuosity of the Intracerebral Vasculature from MRA Images. IEEE-TMI 2003;22:1163–1171.

10. Bullitt E, Jung I, Muller K, Gerig G, Aylward S, Joshi S, Smith K, Ewend M. Determining Malignancy of Brain Tumors by Analysis of Vessel Shape. Lecture Notes in Computer Science. 2004in press

11. Baish JS, Jain RK. Fractals and Cancer. Cancer Research 2000;60:3683–3688. [PubMed: 10919633]

12. Folkman J. Incipient Angiogenesis. Journal of the National Cancer Institute 2000;92:94–95. [PubMed: 10639502]

13. Jain RK. Normalizing Tumor Vasculature with Anti-angiogenic Therapy: A New Paradigm for Combination Therapy. Nature Medicine 2001;7:987–998.

14. Aylward S, Bullitt E. Initialization, Noise, Singularities, and Scale in Height Ridge Traversal for Tubular Object Centerline Extraction. IEEE-TMI 2002;21:61–75.

15. Bullitt E, Aylward S, Smith K, Mukherji S, Jiroutek M, Muller K. Symbolic Description of Intracerebral Vessels Segmented from MRA and Evaluation by Comparison with X-Ray Angiograms. Medical Image Analysis 2001;5:157–169. [PubMed: 11516709]

16. Prastawa M, Bullitt E, Moon N, Van Leemput K, Gerig G. Automatic Brain Tumor Segmen-tation by Subject Specific Modifi-cation of Atlas Priors. Academic Radiology 2003;10:1341–1348. [PubMed: 14697002]

17. Schnabel JA, Rueckert D, Quist M, Blackall JM, Castellano Smith AD, Hartkens T, Penney GP, Hall WA, Liu H, Truwit CL, Gerritsen FA, Hill DLG, Hawkes JD. A Generic Framework for Non-rigid Registration Based on Non-uniform Multi-level Free-form Deformations. MICCAI 2001 Lecture Notes in Computer Science 2001;2208:573–581.

18. Rueckert, D. Review. 2002. Available: www.doc.ic.ac.uk/~dr/software

19. ICBM Atlas. McConnell Brain Imaging Centre, Montréal Neurological Institute, McGill University; Montréal, Canada:

20. Aronen HJ, Gazit IE, Louis DN, et al. Cerebral Blood Volume Maps of Gliomas: Comparison with Tumor Grade and Histologic Findings. Radiology 1994;191:41–51. [PubMed: 8134596]

21. Bruening R, Kwong KK, Vevea MJ, et al. Echo-planar MR Determination of Relative Cerebral Blood Volume in Human Brain Tumors: T1 Versus T2 Weighting. AJNR Am J Neuroradiol 1996;17:831–840. [PubMed: 8733954]

22. Sugahara T, Korogi Y, Kochi M, et al. Correlation of MR Imaging-determined Cerebral Blood Volume Maps with Histologic and Angiographic Determination of Vascularity of Gliomas. AJR Am J Roentgenol 1998;171:1479–1486. [PubMed: 9843274]

23. Sugahara T, Korogi Y, Shigematsu Y, et al. Value of Dynamic Susceptibility Contrast Magnetic Resonance Imaging in the Evaluation of Intracranial Tumors. Top Magn Reson Imaging 1999;10:114–124. [PubMed: 10551626]

24. Shimizu H, Kumabe T, Tominaga T, et al. Noninvasive Evaluation of Malignancy of Brain Tumors with Proton MR Spectroscopy. AJNR Am J Neuroradiol 1996;17:737–747. [PubMed: 8730195]

25. Tedeschi G, Lundbom N, Raman R, et al. Increased Choline Signal Coinciding with Malignant Degeneration of Cerebral Gliomas: A Serial Proton Magnetic Resonance Spectroscopy Imaging Study. J Neurosurg 1997;87:516–524. [PubMed: 9322842]

26. Wilken B, Dechent P, Herms J, et al. Quantitative Proton Magnetic Resonance Spectroscopy of Focal Brain Lesions. Pediatr Neurol 2000;23:22–31. [PubMed: 10963966]

27. Tamiya T, Kinoshita K, Ono Y, et al. Proton Magnetic Resonance Spectroscopy Reflects Cellular Proliferative Activity in Astrocytomas. Neuroradiology 2000;42:333–338. [PubMed: 10872152]

28. Shimizu H, Kumabe T, Shirane R, et al. Correlation Between Choline Level Measured by Proton MR Spectroscopy and Ki-67 Labeling Index in Gliomas. AJNR Am J Neuroradiol 2000;21:659–665. [PubMed: 10782774]

29. Yang D, Korogi Y, Sugahara T, et al. Cerebral Gliomas: Prospective Comparison of Multivoxel 2D Chemical-shift Imaging Proton MR Spectroscopy, Echoplanar Perfusion and Diffusion-weighted MRI. Neuroradiology 2002;44:656–666. [PubMed: 12185543]

30. Law M, Cha S, Knopp EA, et al. High-grade Gliomas and Solitary Metastases: Differentiation by Using Perfusion and Proton Spectroscopic MR Imaging. Radiology 2002;222:715–721. [PubMed: 11867790]

31. Henry RG, Vigneron DB, Fischbein NJ, et al. Comparison of Relative Cerebral Blood Volume and Proton Spectroscopy in Patients with Treated Gliomas. AJNR Am J Neuroradiol 2000;21:357–366. [PubMed: 10696024]

32. Tzika AA, Vajapeyam S, Barnes PD. Multivoxel Proton MR Spectroscopy and Hemodynamic MR Imaging of Childhood Brain Tumors: Preliminary Observations. AJNR Am J Neuroradiol 1997;18:203–218. [PubMed: 9111654]

33. Kelly PJ, Daumas-Duport C, Scheithauer BW, et al. Stereotactic Histologic Correlations of Computed Tomography- and Magnetic Resonance Imaging-defined Abnormalities in Patients with Glial Neoplasms. Mayo Clin Proc 1987;62:450–459. [PubMed: 3553757]

34. Brant-Zawadzki M, Berry I, Osaki L, et al. Gd-DTPA in Clinical MR of the Brain: I Intraaxial Lesions. AJR Am J Roentgenol 1986;147:1223–1230. [PubMed: 3490758]

35. Brant-Zawadzki M, Badami JP, Mills CM, et al. Primary Intracranial Tumor Imaging: A Comparison of Magnetic Resonance and CT. Radiology 1984;150:435–440. [PubMed: 6691098]

36. Bydder GM, Steiner RE, Young IR, et al. Clinical NMR Imaging of the Brain: 140 Cases. AJR Am J Roentgenol 1982;139:215–236. [PubMed: 6979874]

37. Just M, Thelen M. Tissue Characterization with T1, T2, and Proton Density Values: Results in 160 Patients with Brain Tumors. Radiology 1988;169:779–785. [PubMed: 3187000]

38. Felix R, Schorner W, Laniado M, et al. Brain Tumors: MR Imaging with Gadolinium-DTPA. Radiology 1985;156:681–688. [PubMed: 4040643]

39. Moller-Hartmann W, Herminghaus S, Krings T, et al. Clinical Application of Proton Magnetic Resonance Spectroscopy in the Diagnosis of Intracranial Mass Lesions. Neuroradiology 2002;44:371–381. [PubMed: 12012120]

40. Dean BL, Drayer BP, Bird CR, et al. Gliomas: Classification with MR Imaging. Radiology 1990;174:411–415. [PubMed: 2153310]

41. Watanabe M, Tanaka R, Takeda N. Magnetic Resonance Imaging and Histopathology of Cerebral Gliomas. Neuroradiology 1992;34:463–469. [PubMed: 1436452]

42. Kondziolka D, Lunsford LD, Martinez AJ. Unreliability of Contemporary Neurodiagnostic Imaging in Evaluating Suspected Adult Supratentorial (low-grade) Astrocytoma. J Neurosurg 1993;79:533–536. [PubMed: 8410222]

43. Dean BL, Drayer BP, Bird CR, et al. Gliomas: Classification with MR Imaging. Radiology 1990;174:411–415. [PubMed: 2153310]

44. Daumas-Duport C, Scheithauer B, O'Fallon J, et al. Grading of Astrocytomas: A Simple and Reproducible Method. Cancer 1988;62:2152–2165. [PubMed: 3179928]

45. Burger PC, Vogel FS, Green SB, et al. Glioblastoma Multiforme and Anaplastic Astrocytoma: Pathologic Criteria and Prognostic Implications. Cancer 1985;56:1106–1111. [PubMed: 2990664]

46. Burger P. Malignant Astrocytic Neoplasms: Classification, Pathology, Anatomy, and Response to Therapy. Semin Oncol 1986;13:16–20. [PubMed: 3006257]

47. Brey EM, King TW, Johnston C, McIntire LV, Reece GP, Patrick CW. A Technique For Quantitative Three-dimensional Analysis of Microvascular Structure. Microvascular Research 2002;63:279–294. [PubMed: 11969305]
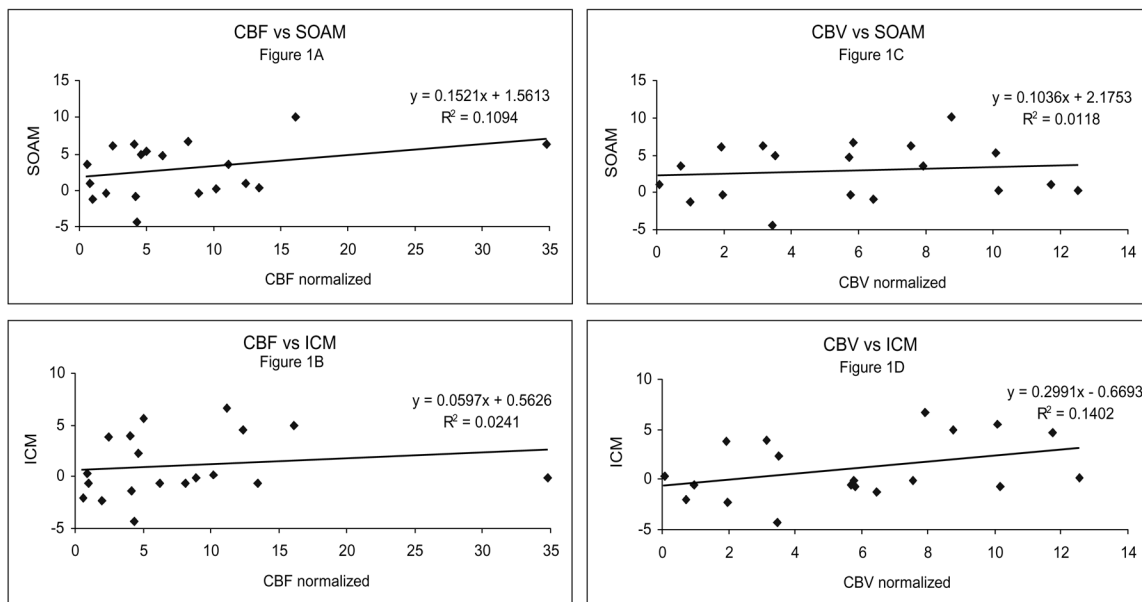
Figure 1.
Linear correlations between (**a**) normalized cerebral blood flow (nlCBF) and the vessel tortuosity parameter Sum of Angles Metric (SOAM); (**b**) nlCBF and the vessel tortuosity parameter Inflection Count Metric (ICM); (**c**) normalized cerebral blood volume (nlCBV) and SOAM; (**d**) nlCBV and ICM are shown. Correlation coefficients are given. hypervascularity are present, will also exhibit abnormalities detectable by the ICM. More information on the mathematical definition of these measures is found in (9).

Table I

	SOAM	ICM
rCBV	$R^2=0.0118$ (p=0.658)	$R^2=0.1402$ (p=0.114)
rCBF	$R^2=0.1094$ (p=0.167)	$R^2=0.0241$ (p=0.526)